Est. 1984

ORIENTAL JOURNAL OF CHEMISTRY
An International Open Access, Peer Reviewed Research Journal

www.orientjchem.org

ISSN: 0970-020 X
CODEN: OJCHEG
2022, Vol. 38, No.(1):
Pg. 144-150

Visible Light Degradation of Rose bengal Dye with a Novel WO_2/α-$ZnMoO_4$ Nanocomposite as Photocatalyst

SUDHAKAR. C[1], DEVI. R[2], NIKHIL. S[1], KARTHIKA. A[3], KALYANI. P[4]*, SUGANTHI. A[3]* and RAJARAJAN. M[4]*

[1]School of Chemistry, Madurai Kamaraj University, Madurai-625021, Tamilnadu, India.
[2]Department of Chemistry, C. P. A. College, Bodinayakanur-625582, Tamilnadu, India.
[3]Department of Chemistry, Thiagarajar College, Madurai-625009, Tamilnadu, India.
[4]Directorate of Distance Education, Madurai Kamaraj University, Madurai-625 021, Tamilnadu, India.
*Corresponding author E-mail: rajarajanchem1962@gmail.com, suganthiphd09@gmail.com

http://dx.doi.org/10.13005/ojc/380118

(Received: October 23, 2021; Accepted: January 10, 2022)

ABSTRACT

The fabrication of WO_2/α-$ZnMoO_4$ nanocomposite using a novel chemical aqueous technique is described in this research. This treatment is mild, easy to use, affordable, and successful. The samples were described using XRD, FT-IR, SEM, EDX, and UV-DRS as they were created. The WO_2/α-$ZnMoO_4$ is seen in the visible portion of the DRS (Diffuse Reflectance Spectroscopy). The structural and morphological features of the generated WO_2/α-$ZnMoO_4$ nanocomposite were examined using SEM. The photocatalytic activity of WO_2/α-$ZnMoO_4$ nanocomposite for the Rose Bengal degradation was investigated in depth under visible light. The WO_2/α-$ZnMoO_4$ nanocomposite had the best photodynamic performance (59 percent to 96 percent of RB degradation). Adsorption of Rose Bengal came next. Using a kinetic pseudo-first order kinetics, the samples' exceptional stability was tested four times under visible light using photodegradation RB. The relationship between structure of the WO_2/α-$ZnMoO_4$ nanocomposite and photocatalytic activity, are investigated. As a result, the method of preparation throws light on the photocatalytic destruction of organic pollutants using WO_2/α-$ZnMoO_4$ nanocomposite.

INTRODUCTION

Heterogeneous photocatalysis has become a popular research topic in recent years. The photocatalytic activities of the nanocomposite powered by visible light have been widely recognized in the degradation of organic molecules and have found increased application in industrial wastewater treatment. While degrading, some colours produce carcinogens and poisonous chemicals that are harmful to all living things. The water-soluble dye Rose Bengal (RB) is extensively used in industries. To extract RB from wastewater, researchers looked at using cheap, non-toxic, large-surface-area, and environmentally acceptable adsorbents. When organic dye-containing effluents are discharged into

the ecosystem, they produce a dark colour and a foul odour. Adsorbents based on nanomaterials are executed for the removal of dyes. These adsorbents have reactive atoms and huge surface area, as well as wide pores, which could be used as a new technique for wastewater treatment[1]. The ternary semiconductor oxide tungsten oxide/zinc molybdate (WO_2/-$ZnMoO_4$) is essential[2]. Because of its excellent electrical and optical properties and benign nature, tungsten oxide/zinc molybdate (WO_2/-$ZnMoO_4$) is an essential inorganic material with a broad range of applications in catalysis, photoluminescence, humidity sensors, anticorrosive paints, battery materials, and photonic crystals. It is a natural inorganic material having two separate crystalline phases: a-triclinic and b-monoclinic. Zinc atoms are bound to six oxygen atoms in the WO_2/-$ZnMoO_4$ triclinic structure, yielding deformed octahedral (ZnO_6) clusters. The tetrahedral clusters (MoO_4) are formed when molybdenum atom is coordinated by four oxygen atoms. The b-$ZnMoO_4$ monoclinic structure, on the other hand, has Mo and Zn atoms together linked to six oxygen atoms, leading the creation of distorted octahedral clusters (ZnO_6)/(MoO_6). Many attempts have been done in the past to investigate the characteristics and preparation of WO_2/-$ZnMoO_4$ nanocomposite from nanometre to micrometre dimensions. These methods, on the other hand, require high temperatures, tedious processes, and the use of organic solvents. Thermal methods have currently been widely used in the preparation and controlling the structure of a variety of oxide materials. Ability to create pure oxides at low temperatures is one of the key advantages of the thermal technique (scale). Dyes are a significant group of chemicals[3] that are commonly released in industrial wastes and then discharged into surface waterways. The dyes may block sunlight from entering rivers, affecting photosynthetic responses. The colours also have an impact on aquatic life and the food chain. Many novel waste water treatment research approaches are being developed in order to protect the environment[4]. During the last few decades, the photocatalysis technique has been successfully used to destroy contaminants. To improve the photocatalytic effectiveness of photocatalysts, extensive research has been done in recent years with new process technologies or different starting materials. As a result, in this study, the synthesis of WO_2/-$ZnMoO_4$ without the use of surfactants was studied utilizing a thermal reaction with $Zn(NO_3)_2 6H_2O$ and $Na_2MoO_4 2H_2O$ as precursors. WO_2/-$ZnMoO_4$ crystals, which operate as a promising visible-light-responsive photocatalyst, also show good activity.

EXPERIMENTAL

Synthesis of WO_2

Under vigorous swirling, 3 g of sodium tungstate ($Na_2WO_4.2H_2O$) was added to 50 mL of distilled water. Drop wise, 12.5 mL of concentrated HCl was added to the aforesaid solution for 30 min of constant stirring. 1.77 g citric acid diluted in 50 mL distilled water was dropped into the aforesaid solution and agitated for 2 hours. The samples were filtered, washed, and dried at 100°C for 2 h before being calcinated at 300°C for 2 hours.

Synthesis of α-$ZnMoO_4$

3 g of ammonium molybdate($(NH_4)_6 Mo_7O_{24}.4H_2O$) was added to distilled water (50 mL) and stirred vigorously for 30 min at 800°C.Then 0.4 g zinc acetate was dissolved drop by drop in 50 mL distilled water. Both the solutions are mixed and rapidly agitated at 80°C for 2 hours. The samples were filtered, washed, and dried at 100°C degrees Celsius for 2 h before being calcinated at 300°C for 2 hours.

Synthesis ofWO_2/α-$ZnMoO_4$ nanocomposite

In 10 mL of ethanol, 4.9 g α-Zinc molybdate (α-$ZnMoO_4$) and 2.4 g of tungsten dioxide (WO_2) were dissolved. The entire mixture was sonicated for 30 min before being stirred continuously for 2 h at ambient conditions. The precipitate filtered with Whatman filter paper and washed with double distillation water and ethanol. In a muffle furnace synthesis of WO_2/α-$ZnMoO_4$ nanocomposite, the samples were dried at 100°C for 1 h before being calcinated at 500°C for 2 hours.

Characterizations

The UV-Vis diffuse reflectance spectra were recorded ranging from 200nm to 800nm using a JASCOV-550 double beem spectrophotometer with PMT detector equipped with an integrating sphere assembly for dry-pressed disk samples, using $BaSO_4$ as reference[5]. The phase and structure of the samples were confirmed by Powder X-ray Diffraction using XPERT PRO X-ray with Cukα radiation at 25°C and structural assignments were in accordance

with the standard JCPDS files. Scanning Electron Microscopy (SEM) images of the nanoparticles were taken by a JM6701F 6701 instrument in both secondary and backscattered electron modes. The elemental analysis was carried out by energy dispersive X-ray spectroscopy (EDX) instrument attached to the SEM[6]. A jacketed cylindrical quarts photoreactor was used to conduct the photocatalytic experiments. Visible light was generated using a 300 W Xenon arc lamp with 420nm cutoff filter to ensure perfect irradiation. By circulating water in the cooling jacket of the photoreactor, the reaction temperature was maintained at 25^{0}C. The Rose Bengal solution including the photocatalyst was magnetically stirred for 30 min in the dark prior to visible light irradiation[7], to ensure the presence of adsorption band at 542nm in the UV-Visible spectra using JASCO UV-Vis spectrometer 530. The photodegradation percentage of Rose Bengal was calculated by the formula given below.

$$\text{Photodegradation (\%)} = C_0\text{-}C/C_0 \text{ X } 10 \quad (1)$$

Where,

C_0-Initial concentration of Rose Bengal.

C-Concentration of the Rose Bengal at time 't'.

RESULTS AND DISCUSSION

Optical Properties

The photocatalytic effectiveness of nanoparticles is largely determined by their optical characteristics. Fig. 1 display the UV- DRS spectra of -$ZnMoO_4$, WO_2, and WO_2/α-$ZnMoO_4$ nanocomposite (a). When WO_2/α-$ZnMoO_4$ nanocomposite was compared to other WO_2 samples, the absorption between 400 and 500nm increased significantly, indicating that the light absorption band was red-shifted. The band gaps were investigated using the Tauc plot.

FT-IR

The FT-IR spectra of α-$ZnMoO_4$, WO_2 and WO_2/α-$ZnMoO_4$ nanocomposite are displayed in Fig. 2. The band at 996 cm^{-1} corresponds to the stretching mode of Mo-O bond, while the peaks at 562 cm^{-1} and 859 cm^{-1} correspond to the stretching modes of oxygen attached with metal atoms (Mo–O–Mo)[8] respectively. The strongest peak at 813 cm^{-1} specified as the doubly connected bridge-oxygen Mo_2–O stretching modes[9]. Two weak vibrations were detected at around 1384 cm^{-1} indicating the vibrational mode of Mo–OH bond and the bending mode of adsorbed water[10]. The absorption peaks at 761 and 890 cm^{-1} are originated from stretching and bending vibrations of ZnOW. The two peaks at 3473 and 1635 cm^{-1} implying the basic hydroxyl group in nanocomposite[11] and also attributed to stretching vibrations of the OH groups in W-OH. The band at 670 cm^{-1} is due to Zn-O bending vibration. Peaks occurred below 610 cm^{-1} belongs to Zn-O band vibrations[12].

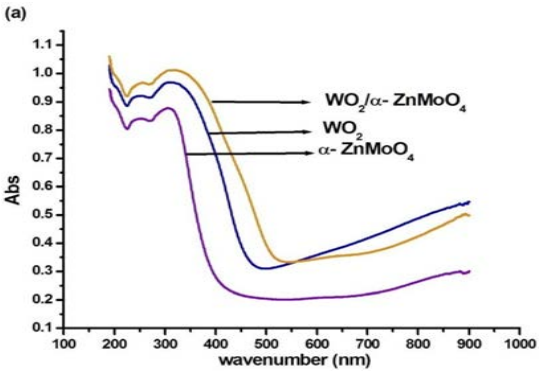

Fig. 1(a). UV-Vis-DRS spectrum of α-$ZnMoO_4$, WO_2 and WO_2/α-$ZnMoO_4$ nanocomposite

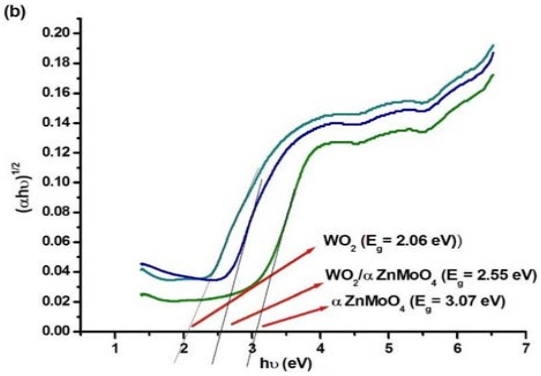

Fig. 1(b). Tauc Plots of α-$ZnMoO_4$, WO_2 and WO_2/α-$ZnMoO_4$ nanocomposite

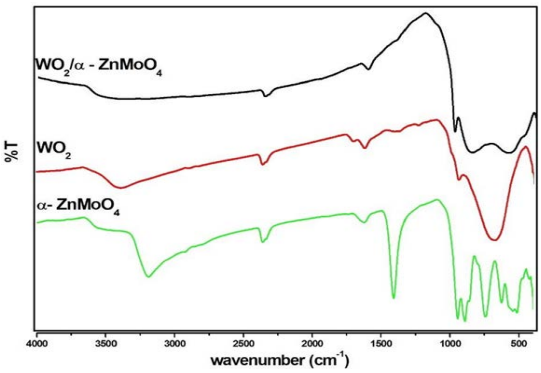

Fig. 2. FT-IR Spectrum of α-$ZnMoO_4$, WO_2 and WO_2/α-$ZnMoO_4$ nanocomposite

Powder XRD Studies

XRD patterns of -$ZnMoO_4$, WO_2, and WO_2/α-$ZnMoO_4$ nanocomposite generated by wet chemical synthesis are shown in Fig. 3. The JCPDS file numbers 350765 (-$ZnMoO_4$) and 860134 correspond to the XRD patterns (WO_2). The diffraction peaks in the XRD pattern of WO_2/α-$ZnMoO_4$ nanocomposite are at 24.3432 (2). Furthermore, the diffraction peaks are more strong and sharper, showing that the produced products have a better crystalline character with smaller particle size. Debye Scherrer's formula, which has been presented below for better understanding, estimated the crystallite size of -$ZnMoO_4$, WO_2, and WO_2/α-$ZnMoO_4$ nanocomposite as 18.99 nm at 2 = 26.6145, 4.09nm at 2 = 25.5497 and 41.62nm at 2 = 24.3432, respectively.

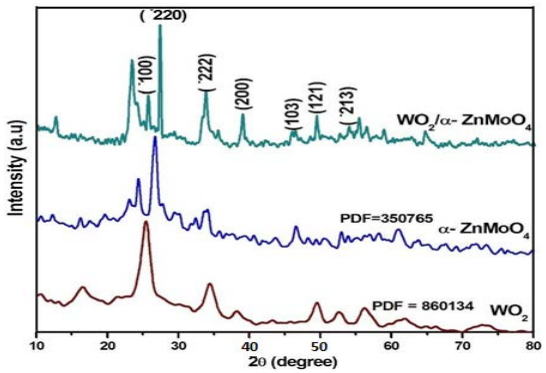

Fig. 3. XRD pattern for α-$ZnMoO_4$, WO_2 and WO^2/α-$ZnMoO_4$ nanocomposite

Morphological studies

The morphological studies of the synthesized compounds were done by Scanning Electron Microscopy and the images are shown in Fig. 4. Fig. 4 (a-c) display SEM images of α-$ZnMoO_4$, WO_2, and WO_2/α-$ZnMoO_4$ nanocompositerespectively. SEM images of α-$ZnMoO_4$ reveals 2D squares, WO_2 reveals nanorods, and the WO_2/α-$ZnMoO_4$ nanocomposite reveals 2D squares with rods. Fig. 5 shows the EDX spectra of α-$ZnMoO_4$, WO_2, and WO_2/α-$ZnMoO_4$ nanocomposite. At their usual energy, the peaks corresponding to W, O, Zn, and Mo are plainly visible.

Photocatalytic activity

UV-Visible Analysis of Rose Bengal Degradation

Under the irradiation of visible light, the WO_2/α-$ZnMoO_4$ nanocomposite catalyst degraded RB with a 96 percent efficiency. The dye degradation increases from 59 percent to 96 percent when the catalyst loading is increased from 0.15 to 0.25 g/L. With a WO_2/α-$ZnMoO_4$ dosage of 0.25 g/L and RB concentration 1 µM, the reaction conditions were tuned, and maximum degradation was achieved in 180 minutes.

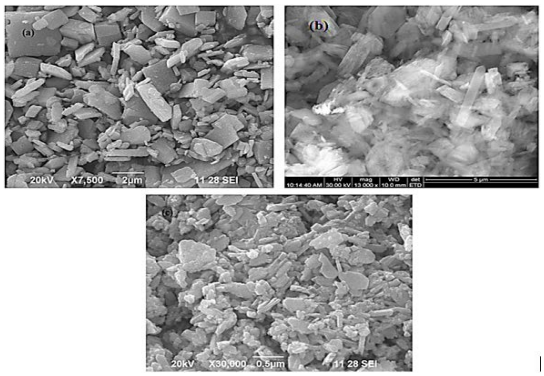

Fig. 4. SEM images of (a) α-$ZnMoO_4$, (b) WO_2 and (c) WO_2/α-$ZnMoO_4$ nanocomposite

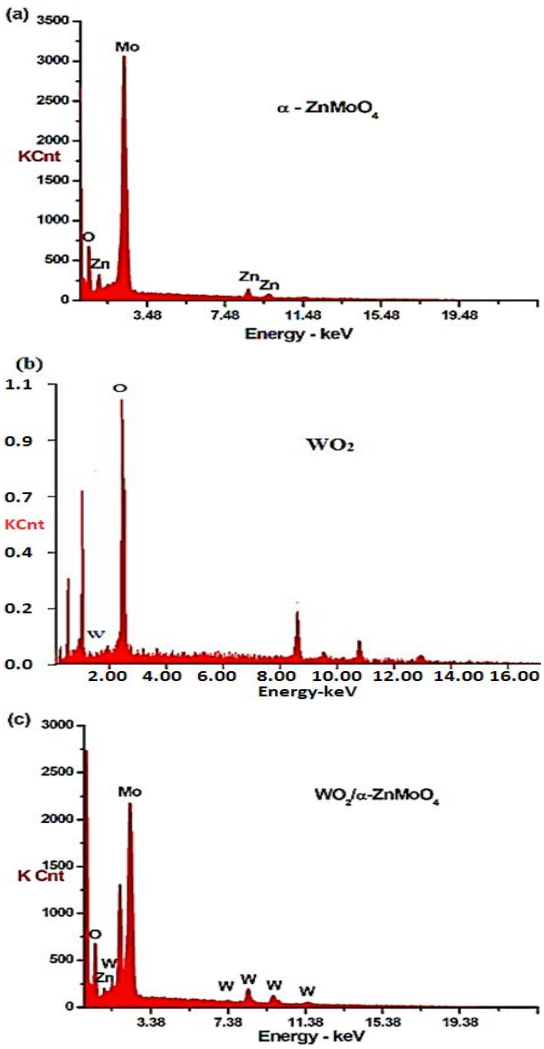

Fig. 5. EDX Spectrum of (a) α-$ZnMoO_4$, (b) WO_2 and (c) WO_2/α-$ZnMoO_4$ nanocomposite

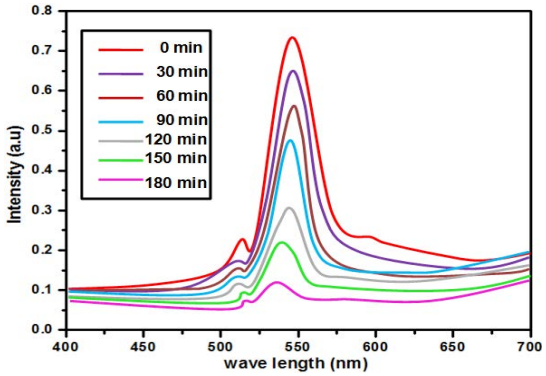

Fig. 6. Comparison of photocatalytic degradation of RB with WO_2/α-$ZnMoO_4$ nanocomposite under the visible light irradiation

Table 1: EDX elemental analysis of α-$ZnMoO_4$, WO_2, WO_2/α-$ZnMoO_4$

Sample	Atomic%	keV
α-$ZnMoO_4$	Zn= 2.87 Mo = 17.35 O = 79.78	Zn= 0.88keV Mo =2.2, 9.8 keVO = 0.52keV
WO_2	W = 28.64 O = 70.82	W = 8.39keV O = 0.5 keV
WO_2/α-$ZnMoO_4$	Zn= 2.87 Mo= 15.01 W = 4.30 O = 77.82	Zn = 0.88 keV Mo= 2.29 W=2.035 keV O = 0.52 keV

Effect of catalyst dosage

By increasing the WO_2/α-$ZnMoO_4$ concentration between 0.15 and 0.30 g/L while keeping the other reaction parameter (RB concentration 1 µM) constant, the effect of photocatalyst concentration on RB degradation was investigated[13]. The dye degradation increased from 59 percent to 96 percent when the catalyst loading was increased from 0.15 to 0.25 g/L[14]. This is because, the active sites on the catalyst's surface increases with the catalyst loading, which enhances the absorption of RB[15]. As a result, the proportion of degradation rises. With a large amount of catalyst the degradation percentage of RB was reduced as the photocatalyst dosage was increased from 0.25 to 0.30 g/L. This could be due to an excessive amount of catalyst obstructing and preventing the penetration of light[16]. Particle aggregation was substantial at high photocatalyst concentrations, reducing the number of active sites on the catalyst surface and lowering the degradation efficiency. It should be emphasized that in the absence of photocatalyst, no substantial degradation of RB was detected.

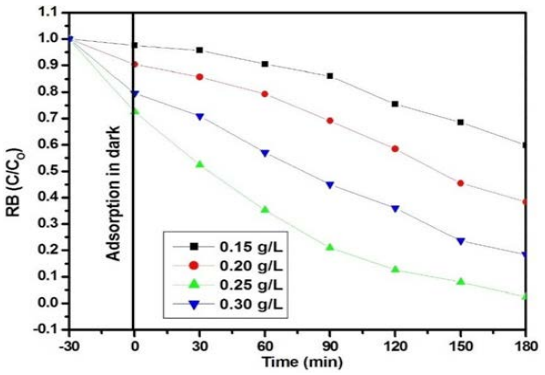

Fig. 7. Effect of WO_2/α-$ZnMoO_4$ nanocomposite dosage on the photodegradation of RB

Effect of initial concentration of Rose Bengal

How the initial concentration of dye affect the breakdown of RB is shown in Fig. 8. When the initial dye concentration (1-3 µM) is increased, the photodegradation of RB diminishes. The production of hydroxyl radicals affects photodegradation efficiency. The adsorbed organic compounds on the surface of the catalyst increase as the initial concentration increases, and the solution becomes more strongly coloured. As a result, there will be fewer active sites for OH adsorption, and hence OH production will be reduced[17]. As the concentration of RB rises, the distance travelled by photons incoming into the aqueous RB solution shortens thus lowering the catalytic efficiency[15].

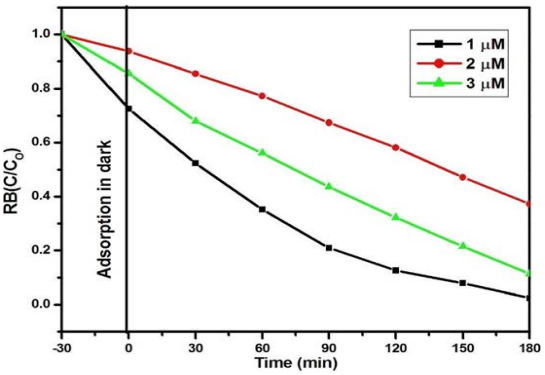

Fig. 8. Effect of initial concentration of RB

Photodegradation kinetics of Rose Bengal

The kinetics of RB photocatalytic degradation were studied under optimum reaction conditions [WO_2/α-$ZnMoO_4$ nanocomposite = 0.25g/L, pH7, RB = 1µM]. Fig. 9 depicts the kinetic course of degradation of RB. The photocatalytic degradation of RB obeys pseudo-first order kinetics, and the reaction can be given as

$$-\ln(C/C_o) = kt \quad (2)$$

Where

C_o = initial concentration of RB at = 0 min,

C = concentration of RB at time 't',

k = Rate constant.

The plot of –ln (C/C_o) vs irradiation time't' in Fig. 9 revealed a linear relationship. The rate constant is calculated by using the slope of the '–ln (C/C_o) against time' plot. The rate constant (k) for α-$ZnMoO_4$, WO_2 and WO_2/α-$ZnMoO_4$ nanocomposite was estimated from the slopes and found to be 1.857 x 10^{-2} s^{-1}, 9.27 x 10^{-3} s^{-1} and 6.64 x 10^{-3} s^{-1}, respectively.

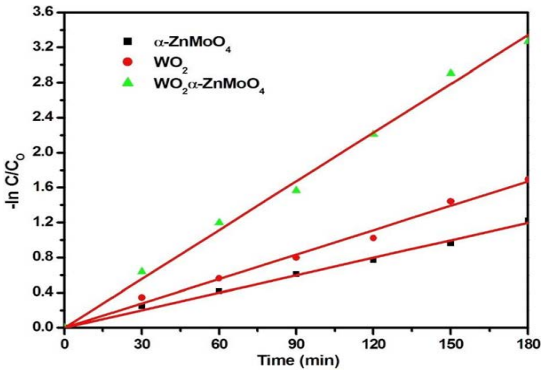

Fig. 9. Kinetic plot of –ln(C/C_o) vs irradiation time

Table 2: Analytical comparison of various previously reported photocatalysts with our present catalyst

S. No	Dye	Catalyst	Percentage	References
1	Rose Bengal	PANI–SWCNT	95.91%	18
2	Rose Bengal	Ag/CeO_2	96%	19
3	Rose Bengal	samarium doped CeO_2	89%	20
4	Rose Bengal	g-C_3N_4/ZnO	90%	21
5	Rose Bengal	iron doped NiO	86%	22
6	Rose Bengal	Zirconium Doped Copper Ferrite ($CuFe_2O_4$)	88%	23
7	Rose Bengal	PJ-AgNPs	83%	24
8	Rose Bengal	WO_2/α-$ZnMoO_4$	96%	Present work

CONCLUSION

In the current work, we have developed a novel WO_2/α-$ZnMoO_4$ nanocomposite possessing high visible light photocatalytic activity. The nanocomposite was synthesized via a co-precipitation method. The WO_2/α-$ZnMoO_4$ nanocomposite is compact and homogenous, with 2D squares comprising rod nanoparticles with diameters of roughly 41.62nm, according to the findings. Optical investigations revealed that the band gap of the WO_2/α-$ZnMoO_4$ nanocomposite is 2.55 eV. The photocatalyst WO_2/α-$ZnMoO_4$ nanocomposite was successfully employed for the degradation of RB. The improved photocatalytic activity of the WO_2/α-$ZnMoO_4$ nanocomposite was due to the inhibition of electron-hole recombination. Using a 0.25 g/L WO_2/α-$ZnMoO_4$ nanocomposite with a 1 µM RB concentration, maximum photodegradation (96%) was achieved in 180 minutes. The WO_2/α-$ZnMoO_4$ nanocomposite increased optical properties, surface conformity, photocatalytic activity, and stability, according to the findings.

ACKNOWLEDGEMENT

The authors thank School of Chemistry, Madurai Kamaraj University for providing all the facilities for conducting this research work.

Conflict of Interest

The authors declare that there is no conflict of interests regarding the publication of this article.

REFERENCES

1. Ramasamy Raja V.; Rani Rosaline D.; Suganthi A.; Rajarajan M.; *Ultra. S. Chem.* **2018**, *44*, 310-318.
2. Alpuche-Aviles M.A.; Wu Y.; *J. Am. Chem. Soc.*, **2009**, *131*, 3216-3224.
3. Bayati. F.; Golestani-Fard.; Moshfegh. AZ.; *Cat. Let.*, **2010**, *134*, 162-168.
4. Yu-Rou M. R.; Jiang, Wenlian William Lee.; Kung-Tung Chen.; Ming-Chien Wang.; Ken-Hao Chang.; Chiing-Chang Chen.; *J. Tai. Inst. Chem. Eng.*, **2014**, *45*, 207-218.
5. Arunadevi. R.; Kavitha. B.; Rajarajan. M.; Suganthi. A.; *Sep Sci Tech.,* **2018**, *53*, 2456-2467.
6. Vignesh. K.; Priyanka. R.; Rajarajan. M.; Suganthi. A.; *Mat. Sci. Eng*: B., **2013**, *78*, 149-157.

7. Arunadevi. R.; Kavitha. B.; Rajarajan M.; Suganthi. A.; Jeyamurugan. A.; *J. Surf. Inter.*, **2018**, *10*, 32-44.
8. He, Yiming.; Lihong Zhang.; Xiaoxing Wang.; Ying Wu.; Hongjun Lin.; Leihong Zhao.; Weizheng Weng.; Huilin Wan, and Maohong Fan, *J. RSC Adv.*, **2014**, *4*, 13610–13619.
9. Mancheva. M.; Iordanova. R.; Dimitriev. Y.; *J. Alloy. Comp.*, **2011**, *509*, 15.
10. Zakharova. G.S.; Taschner. C.; Volkov. V.L.; *Sol. St. Sci.*, **2007**, *9*, 1028.
11. Komarneni. S.; Roy. R.; Li. Q.H.; *Mat. Res. Bull.*, **1992**, *27*, 1393.
12. Sajjad, Ahmed Khan Leghari, SajjadShamaila, and Jinlong Zhang., *J. Haz. Mat.*, **2012**, *235*, 307-315.
13. Liu. G.; Liao. S.; Zhu. D.; Cui. J.; Zhou. W.; *Sol. St. Sci.*, **2011**, *46*, 1295.
14. Vignesh. K.; Priyanka. R.; Hariharan. R.; Rajarajan. M.; Suganthi. A.; *J. Ind. Eng. Chem.*, **2014**, *20*, 435-443.
15. Buvaneswari. K.; Karthiga. R.; Kavitha. B.; Rajarajan. M.; Suganthi. A.; *Appl. Surf. Sci.,* **2015**, *356*, 333-340.
16. Yeung. K.L.; Yau. S.T.; Maira. A. J.; Coronado. J. M.; Soria. J.; Yue. P. L.; *J. Catal.,* **2003**, *219*, 107.
17. Lu. X.; Song. C.; Jia. S.; Tong. Z.; Tang. X.; Teng. Y.; *Chem. Eng. J.*, **2015**, *260*, 776.
18. Mukulika Jana Chatterjee.; Amrita Ghosh.; Anup Mondal.; Dipali.; *RSC Adv.*, **2017**, *7*, 36403.
19. Murugadoss, G.; Dinesh Kumar. D.; Rajesh Kumar. M.; Venkatesh. N.; Sakthivel. P.; *Sci. Rep.*, **2021**, *11*, 1-13.
20. Chahal. S.; Rani. N.; Kumar. A.; Kumar. P.; *Vacuum.,* **2020**, *172*, 109075.
21. Alharthi. A.; Alghamdi. A.; Alanazi. HS.; Alsyahi. AA.; *Catalysts.,* **2020**, *10*, 1457.
22. Amita Khatri. P.; Rana. S.; *Phy. B: Con. Mat.*, **2020**, *579*, 411905.
23. Nancy Dayana. P.; John Abel. M.; Fermi Hilbert Inbaraj. P.; Sivaranjani. S.; Thiruneelakandan. R.; Joseph prince. J.; *Springer Nature.,* **2021**.
24. Malini. S.; VigneshKumar. S.; Hariharan. R.; Pon Bharathi. A.; RenukaDevi P.; Hemananthan Antibacterial. E.; *Mat. Today: Proc.*, **2020**, *21*, 828-832.